RSC Advances

ROYAL SOCIETY OF CHEMISTRY

www.rsc.org/advances

Simple electrochemical synthesis of an Au-Ag-Cu trimetallic nanodendrite and its use as a SERS substrate

Kyeol Chang and Hoeil Chung*

Analytical Spectroscopy Lab, Department of Chemistry and Institute for Materials Design, Hanyang University, Seoul 133-791, Korea. E-mail l address: hoeil@hanyang.ac.kr (H. Chung).

*: Corresponding author

An Au-Ag-Cu trimetallic nanodendrite was constructed by simple electrochemical methods and was evaluated as a surface enhanced Raman scattering (SERS) substrate. The motivation was to harmonize the individual merits of each SERS-active metal, the higher SERS efficiency of Ag, good surface stability of Au, and structural stability of Cu, in a single structure. For the fabrication, a Cu flower-like nanostructure was initially constructed by reduction of Cu^{2+} (electrodeposition). Next, a galvanic replacement reaction (GRR) was performed on the Cu framework in a solution of Ag^{+} to build Ag nanodendrites with coincidental release of Cu atoms into the solution as Cu^{2+}. As the Ag nanodendrite grew, released Cu^{2+} redeposited, so a Ag-Cu bimetallic nanodendrite started to form. Next, a second GRR was performed with the newly prepared Ag-Cu nanodendrite in Au^{3+} solution to partially replace Ag and Cu by Au to construct the Au-Ag-Cu trimetallic nanodendrite. Based on examination of Raman peaks of rhodamine 6G (R6G, a reporter molecule), the Ag-Cu nanodendrite resulted in approximately 2.6 fold higher peak intensity compared to a Ag nanodendrite. Subsequent Au incorporation into the Ag-Cu nanodendrite greatly improved the stability of SERS measurements as well as increased the peak intensity further by 7.6 fold, thereby enabling the observation of Raman peaks of a 10^{-10} M R6G sample.

1 Introduction

Recently, SERS has been widely utilized for the analysis of diverse samples to take advantage of its ultra-sensitivity originating from resonance of molecules with a generated local plasmon on the surface of SERS substrates.[1-11] Since the substrate is a crucial element governing the sensitivity and reproducibility of SERS measurements, various nanostructured substrates such as particles,[12-17] rods,[18-25] stars,[26-30] and dendrites[31-41] composed of Ag, Au, or Cu have been extensively developed to fulfill the necessary requirements. Nanostructures of bi-metallic composition have also been studied in parallel due to their unique and useful properties unobtainable from mono-metallic structures including Au-Ag, Cu-Ag, and Au-Cu bimetallic coreshells,[42-48] dendrites,[49-56] and other structures,[57-63] as well as their improved SERS efficiencies in comparison with mono-metallic structures.

Along with the development of bimetallic nanostructures, exploration of trimetallic structures has also

grown with the hope of further performance improvement by incorporation of an additional element, such as porous Ag/Au/Pt nanocages,[64] Au/Pd/Pt colloidal nanocomposites,[65] and Au/Pt/Ag nanocomposites[66,67] used for SERS measurements of rhodamine 3B, l-cysteine, and 7-azaindole, respectively. Alternatively, trimetallic structures incorporating all three SERS-active elements of Ag, Au, and Cu in a single unit to integrate the individual merits of each metal, the higher SERS activity of Ag,[13, 15-19, 25, 27, 28] better surface stability of Au,[12-17, 20-26, 29, 30] and structural stability of Cu,[16, 17, 25] have been demonstrated. Examples of such structures include Au-Ag-Cu nanocrystals fabricated by a three-step chemical reduction[68] and Au-Ag-Cu particles synthesized through a polyol method.[69] The structures and optical properties of these trimetallic were well characterized.

A substrate possessing a larger number of hotspots with a high surface-to-volume ratio is greatly beneficial for SERS measurements. In this context, a nanodendrite structure is promising since it has a hierarchical structure with a large population of edges as well as acute angles in terraces. Therefore, in this work, we attempted to fabricate an Au-Ag-Cu trimetallic nanodendrite by simple electrochemical methods rather than complex chemical methods, requiring several synthetic steps involving a long period of reaction time as well as extensive use of chemicals, and to evaluate it as a SERS substrate. Initially, a Cu flower-like nanostructure possessing a large surface area was constructed by reduction of Cu^{2+} (electrodeposition) and used as a framework to easily host Ag and Au, since the reduction potential of Cu is lower than those of Ag and Au. Also, Cu-based nanostructure was stable, so homogeneous incorporation of a subsequent metal such as Ag into it was realized as reported.[16, 17, 25] This was one of main causes for employing Cu frame to build a trimetallic structure. A galvanic replacement reaction (GRR) was then performed on the Cu flower-like framework in a solution of Ag^{+} to build a Ag nanodendrite structure with concurrent release of Cu atoms into the solution as Cu^{2+}. As the Ag nanodendrite grew, released Cu^{2+} was also redeposited to form a Ag-Cu bimetallic nanodendrite structure.[49, 56] Next, a second GRR was performed with the Ag-Cu nanodendrite in a solution of Au^{3+} to partially replace Ag and Cu in the structure with Au to construct the Au-Ag-Cu trimetallic nanodendrite. This was to compensate the surface instability of Ag for more reproducible SERS measurements. In each step, the structures of the nanodendrites were characterized by examining the corresponding SEM and TEM images with elemental mappings. The SERS efficiencies of the nanodendrites were examined using R6G as a Raman reporter molecule, and an optimal atomic composition of the Au-Ag-Cu nanodendrite providing the maximum intensity was searched, and the intensity was compared with those obtained with the mono- and bi-metallic nanodendrites. Finally, the Au-Ag-Cu nanodendrite was used to measure R6G samples in the concentration range from 10^{-10} to 10^{-4} M to assess the sensitivity, and the peak intensities of the 10^{-4} M R6G sample measured over 25 days were analyzed to examine the long-term stability.

2 Experimental

2.1. Chemicals and materials

$AgNO_3$ (99.9 wt%, Alfa Aesar) and $HAuCl_4$ (99.9 wt%, Sigma–Aldrich) were used to prepare 10 mM Ag and 5 mM Au galvanic displacement plating solutions, respectively. Other chemicals used in this study,

$CuSO_4$ (Yakuri Pure Chemicals), H_2SO_4 (J.T. Baker), HNO_3 (Daejung Chemicals, Korea), and HCl (Daejung Chemicals), were of analytical grade. High-purity copper foil (99.9 wt%) was purchased from the Nilaco Corporation (Tokyo, Japan). R6G purchased from Sigma–Aldrich was used to prepare a 1 mM R6G stock solution in ethanol (99.5%, Daejung Chemicals). R6G samples with different concentrations (10^{-10} to 10^{-4} M) were prepared by dilution of the stock solution just before SERS measurements.

2.2. Fabrication of the Cu flower-like framework, Ag-Cu and Au-Ag-Cu nanodendrites

A Cu flower-like framework was initially fabricated according to a literature procedure.[36, 40] High-purity Cu foil (0.7 cm × 2.0 cm) was consecutively cleaned with ethanol, dilute nitric acid (1.2 mM), and doubly distilled water (DDW) before use as a cathode for Cu deposition. A Pt electrode was used as the counter electrode (anode). The distance between the two electrodes was kept at 0.5 cm, and a constant potential of -800 mV was applied to the electrodes using a galvanostat (Epsilon, Bioanalytical Chemistry Systems, Inc., USA) over 3 to 12 minutes in an electrolyte solution containing 0.5 M H_2SO_4 and 10 mM $CuSO_4$. The constructed structures were rinsed several times with DDW and ethanol.

The freshly prepared Cu flower-like framework was immediately immersed in a 10 mM $AgNO_3$ solution to initiate GRR with continuous stirring. The reaction was kept in the dark to avoid potential Ag photo-reduction during the entire procedure. The duration of GRR was varied from 2 to 15 minutes to prepare Cu-Ag nanodendrites of varying atomic compositions. The constructed nanodendrites were rinsed with water and dried in air. To make Au-Ag-Cu nanodendrites, the Ag-Cu nanodendrite was dipped in a 2 mL solution of 5 mM $AuCl_4$, and GRR to incorporate Au by releasing Ag and Cu was executed with continuous stirring. The duration of GRR was varied from 5 to 25 s to yield trimetallic nanodendrites with different atomic compositions. An overall schematic of experimental setup and nanodendrite formation is shown in Figure S1 in Electronic Supplementary Information (ESI).

2.3. Structural characterization of nanodendrites

Scanning electron microscope (SEM) images of the fabricated nanodendrites were acquired using a Hitachi S-4800 SEM instrument. Transmission electron microscope (TEM), high-resolution TEM (HRTEM) images, and energy dispersive X-ray (EDX) spectra were obtained on a JEM-2100F transmission electron microscope (JEOL, Japan) with an accelerating voltage of 200 kV. Acquisition time and bin size for EDX mapping was 1520 s and 4.88 nm, respectively. X-ray photoelectron spectroscopy (XPS) was also used to characterize the nanodendrites using an Al·K·α X-ray source (Theta Probe Base System, Thermo Fisher Scientific Co.). SERS spectra were collected using a dispersive Raman microscope equipped with a diode laser (λ = 785 nm, power: 40 mW) and a CCD detector (Kaiser Optical Inc., USA). The size of laser illumination was approximately 10 μm in diameter and power density was 2.04×10^{-2} mW/mm^2.. R6G-adsorbed nanodendrites were positioned on a microscope stage, and the laser beam was focused using an objective lens (10×/0.25NA) to

collect SERS spectra with a resolution of 4 cm^{-1}. In each case, 5 substrates were separately prepared for evaluation and Raman spectra were acquired by randomly illuminating laser at 5 different spots on each substrate with an exposure time of 20 s.

3 Results and discussion

3.1. Fabrication of Ag-Cu nanodendrites and examination of SERS performance

A Cu framework with a flower-like structure was initially constructed through the electrodeposition of Cu on Cu foil by applying a potential of -800 mV as described earlier.[36, 40] Figure 1 shows SEM images of the Cu flower-like structures constructed with increasing duration of electrodeposition (3 (a), 5 (b), 7 (c), 10 (d), and 12 minutes (e)). Structure growth was clearly observable as the electrodeposition proceeded, and an electrodeposition of 10 minutes produced the most distinct flower-like framework possessing the largest surface area, potentially making subsequent electrochemical reactions more efficient for construction of subsequent nanostructures. Electrodeposition longer than 10 minutes made the edges blunt and the overall structure less characteristic. Therefore, the Cu flower-like structure prepared with a 10 minute electrodeposition was used as the framework for further incorporation of Ag and Au. Figure 1 (f) shows a SEM image of the Cu flower-like structure constructed with a 10 minute electrodeposition in a larger field of view. Flower-like structures were widely formed over the surface without local agglomeration or aggregation. Visible extinction spectrum of the corresponding flower-like structure is shown in Figure S2 (refer to Electronic Supplementary Information (ESI)), in which the broad plasmonic band centered at 590 nm is observable.

To generate Ag-Cu nanodendrites, a galvanic replacement reaction (GRR) able to incorporate Ag into the Cu flower-like framework with simultaneous release of Cu was performed in a 10 mM Ag^{+} solution. Figure 2 shows SEM images of Ag-Cu structures obtained by increasing the duration of GRR up to 15 minutes (2 (a), 5 (b), 7 (c), 10 (d), 12 (e), and 15 minutes (f)). During the initial 2-5 minutes of the GRR, Ag-based structures started to form on the framework, while the overall shape of the Cu flower-like structure remained. A 7 minute GRR induced the generation of small nanodendrite structures, which became larger and most characteristic in shape with a 10 minute GRR. When the replacement reaction was preformed longer than 10 minutes, the edges became blunt (12 minutes), and some agglomerated structures such as round dish-like particles started to appear with the 15 minute GRR. When the reaction proceeded longer than 10 minutes, the concentration of Cu^{2+} substantially elevated. The increased Cu^{2+} concentration made replating of Cu faster and so induced the growth of nanodendrite less characteristic such as blunt edge or agglomerated, thereby degrading SERS efficiency of substrates, as also observed in other reports. [30, 51, 70, 71] In addition, visible extinction spectrum of the Ag-Cu nanodendrite built with 10 minute of GRR is shown in Figure S2. As shown, overall spectral feature is extensively broad over the 620-900 nm range without appearance of distinct peaks. The large variation in the sizes of nanodendrites as shown in the SEM image was responsible for the broad extinction band.

Using the Ag-Cu nanodendrites shown in Fig. 2, SERS spectra of R6G (100 μM) were collected as shown in Figure 3 (a). A SERS spectrum of the same R6G sample acquired using the Cu flower-like frame is also displayed (the black spectrum, designated as “0 min” in the legend). The baselines of spectra were corrected at 1700, 1395, 1245, 1100, 980, 690, 530, and 471 cm^{-1}. For comparison, normal Raman spectrum

collected from a 50 mM R6G sample is shown in Figure S3 in ESI. Major bands centered at 1649, 1510, 1363, 773, and 610 cm^{-1} are apparent as has previously been reported.[55] The bands at 1649, 1510 and 1363 cm^{-1} are arisen from the aromatic stretching vibrations. The 773 and 610 cm^{-1} bands are assignable to an out-of-plane bending and an in-plan bending motion of C-C-C ring, respectively. Fig. 3 (b) and (c) highlight the strongest 1510 cm^{-1} peaks and variation of the corresponding peak intensities according to duration of the GRR. Five substrates were separately prepared for each case, and 5 spectra were collected from each substrate by randomly illuminating laser on 5 different spots; therefore, the calculated error bars in Fig. 3 (c) were based on a total of 25 observations. Initiation of the GRR led to increased peak intensity by incorporation of Ag, and the 10 minute GRR provided the strongest intensity due to formation of the most perfect nanodendrite structure, as shown in Fig. 2 (d). As expected, nanodendrites prepared with GRRs longer than 10 minutes led to decreased intensity due to formation of less SERS-efficient structures.

Using the optimal substrate, Raman spectra were consecutively collected at the same location (15 times) and the resulting intensities were examined to find potential occurrence of photo-bleaching of R6G. There was no significant variation in the intensities, thereby confirming no photo-bleaching of R6G during the measurements. Further, Raman spectra of a 100 uM R6G dispersed on flat Cu as well as Ag films were measured for comparison as shown in Figure S4 in ESI. As shown, the intensities were much smaller (approximately 1.1×10^3 times) compared to that acquired using the optimal Ag-Cu nanodendrite.

The atomic composition of the optimal Ag-Cu nanodendrite, determined using EDX analysis by calculating the ratios of corresponding peaks, was 72.4 wt% Ag and 27.6 wt% Cu. Interestingly, a considerable amount of Cu was present in the structure. The Cu^{2+} released into solution from the Cu framework at the earlier stage of GRR was reduced again to regenerate Cu nanoparticles (CuNPs) along with Ag nanodendrite formation based on the primary battery mechanism.[49] In this manner, new Ag-Cu structures were formed in which CuNPs were deposited on the surface of Ag nanodendrites. Thus, the Cu framework also functioned as a Cu source for construction of the Ag-Cu nanodendrite. Figure 4 (a) shows a TEM image of the Ag-Cu nanodendrite (constructed with a 10 minute GRR) and the corresponding elemental mappings of Ag (b), and Cu (c). Nanodendrites carefully detached by a cutter blade were dispersed in acetone, and the resulting solution was dropped and dried on a grid for TEM measurement. In the Ag and Cu mappings, the corresponding colors were uniformly distributed over the structure, thereby confirming homogeneous Ag-Cu alloy formation over the nanodendrite. In addition, an Ag nanodendrite structure prepared by also electrodeposition in our previous reports[51, 52] was used to measure the same R6G sample. The obtained peak intensity (also shown in Fig. 3 (c)) was 2.6 fold lower than that acquired using the Ag-Cu nanodendrite. This result indicates that formation of the bi-metallic Ag and Cu structure is helpful in enhancing SERS efficiency. As reported by several research groups, this enhancement can most probably be attributed to the further roughened surface as well as the occurrence of pinholes induced during formation of the Ag-Cu alloy, which function as SERS hotspots.[33, 49, 53, 54, 56] The roughen surface can be observed in TEM image acquired from an another Ag-Cu nanodendrite as shown in Figure S5 in ESI.

3.2. Fabrication of Au-Ag-Cu nanodendrites and examination of SERS performance

Since the Ag-Cu nanodendrite contained a large amount of Ag, its surface stability would be unsatisfactory for reproducible SERS measurements due to facile formation of an oxide layer on the Ag surface. Therefore, to obtain better surface stability and simultaneously enhance SERS efficiency, incorporation of Au into the Ag-Cu nanodendrite was attempted using a GRR. Since the reduction potentials of Au, Ag, and Cu are 1.52, 0.80, and 0.52 V, respectively, replacement of Cu by Au is relatively more favorable than by Ag. Figure 5 (a) shows the intensities of the 1510 cm^{-1} band acquired using Au-Ag-Cu nanodendrites constructed with five different durations of GRR (5, 10, 15, 20, 25 s). The intensities acquired using the Ag and Ag-Cu nanodendrites (Black square, designated as "0 sec" in the legend) are also shown. The calculated error bars were also based on a total of 25 observations in each case, as described in Fig. 3 (c).

The initiation of Au incorporation into the Ag-Cu nanodendrite led to increased peak intensity at the early stages of GRR. A GRR of 15 s resulted in the strongest intensity, which steeply decreased with longer GRR. This result showed that the addition of an optimal amount of Au into the Ag-Cu structure was effective in further enhancing SERS efficiency, although Au is known to be a less SERS-efficient metal. The atomic composition of Au, Ag, and Cu in the optimal Au-Ag-Cu nanodendrite determined by EDX analysis was 1.58, 76.85, and 21.57 wt%, respectively. As expected, the concentration of Cu in the Au-Ag-Cu nanodendrite was lower compared with the Ag-Cu structure due to the greater release of Cu, which has the lowest reduction potential among the three elements. The co-presence of these three metals in the nanodendrite was also confirmed by observing XPS spectra (refer to Figure S6 in ESI).

Figure 5 (b) shows a SEM image of the optimal Au-Ag-Cu nanodendrite. Many small dots corresponding to Au nanoparticles (AuNPs) on the Ag-Cu nanodendrite are observable. The formation of AuNPs on the surface could accompany the generation of pinholes, since Ag atoms generally segregate on the surface and Au atoms lie in the subsurface of the structure due to their different surface energies (Ag: 78 $meVA^{-2}$, Au: 97 $meVA^{-2}$).[72, 73] Therefore, the observed enhancement largely originates from hotspots induced by pinholes as well as the further roughened surface by formation of the tri-metallic alloy.[48, 55, 72, 73] The roughen surface can be observed in TEM image acquired from an another Au-Ag-Cu nanodendrite as shown in Figure S7 in ESI. Visible extinction spectrum of the optimal Au-Ag-Cu nanodendrite is shown in Figure S2. The overall spectral feature was similar to that of the optimal Ag-Cu nanodendrite. Figure 6 shows a TEM image of the Au-Ag-Cu nanodendrite (a) and the corresponding elemental mappings of Au (b), Ag (c), and Cu (d). Again, each metal was widely present over the structure without noticeable localization as shown by the individual color distributions.

To evaluate the stability of substrates for SERS measurement, a 10 μL R6G sample (10^{-4} M) was applied to the optimal Ag-Cu and Au-Ag-Cu nanodendrites, and Raman spectra of these R6G-adsorbed nanodendrites collected over a period of 25 days were compared, as shown in Figure 7 (a). The error bars were calculated based on a total of 25 observations using 5 separate substrates in each case. The intensities acquired from both nanodendrites decreased over time; however, the decrease was more substantial for the Ag-Cu nanodendrite yielding a 61.1% intensity decline over 25 days compared to the original intensity, while the

decline was 35.2% in the case of the Au-Ag-Cu nanodendrite. Another notable observation was that the magnitudes of the error bars were much greater for the Ag-Cu nanodendrite based measurements, clearly indicating inferior surface stability. The average of relative standard deviations (RSDs) of each measurement using the Ag-Cu and Au-Ag-Cu nanodendrites was 26.3% and 2.6%, respectively. The incorporation of Au clearly improved the reproducibility of SERS measurements.

Finally, using the Au-Ag-Cu nanodendrite, Raman spectra of seven R6G samples with concentrations ranging from 10^{-10} to 10^{-4} M were acquired, as shown in Figure 7 (b). The inset presents the intensities acquired from samples of the two lowest concentrations (10^{-9}, and 10^{-10} M). As shown, the intensity increased with the elevation of R6B concentration, and the major R6G peaks were sufficiently observed even with the 10^{-10} M sample.

4 Conclusions

The first reported Au-Ag-Cu trimetallic nanodendrite was successfully fabricated via electrodeposition and GRRs, much simpler procedures than chemical synthetic methods. The incorporation of Au into the Ag-Cu nanodendrite was successful in ensuring the reproducibility of subsequent SERS measurements as well as increasing the SERS intensity. In comparison with the intensity obtained using the Ag nanodendrite, the Au-Ag-Cu nanodendrite provided 14.2 fold greater intensity, thereby enabling the observation of Raman peaks for a 10^{-10} M R6G sample. We believe that multi-metal incorporated nanostructures are versatile substrates for SERS and electrochemical measurements, as well as for catalysts. Other than the nanodendrite structure, for multi-purpose applicability, more structurally effective materials composed of multi-metallic alloys are under development.

Acknowledgements

This research was supported by Basic Science Research Program through the National Research Foundation of Korea (NRF) funded by the Ministry of Science, ICT and Future Planning (2015R1A2A2A01006445).

Notes and references

1. A. Campion and P. Kambhampati, *Chem. Soc. Rev.*, 1998, **27**, 241-250.
2. R. L. Garrell, *Analytical Chemistry*, 1989, **61**, 401A-411A.
3. C. L. Haynes, A. D. McFarland and R. P. V. Duyne, *Analytical Chemistry*, 2005, **77**, 338 A-346 A.
4. C. J. Hicks, *MSU CEM*, 2001, **924**.
5. S. Jiang, *Term Paper for Physics*, **598**.
6. K. Kneipp, Y. Wang, H. Kneipp, L. T. Perelman, I. Itzkan, R. R. Dasari and M. S. Feld, *Physical review letters*, 1997, **78**, 1667.

7. M. Moskovits, *Journal of Raman Spectroscopy*, 2005, **36**, 485-496.
8. B. Sharma, R. R. Frontiera, A.-I. Henry, E. Ringe and R. P. Van Duyne, *Materials today*, 2012, **15**, 16-25.
9. P. L. Stiles, J. A. Dieringer, N. C. Shah and R. P. Van Duyne, *Annu. Rev. Anal. Chem.*, 2008, **1**, 601-626.
10. U. K. Sur, *Resonance*, 2010, **15**, 154-164.
11. K. A. Willets and R. P. Van Duyne, *Annu. Rev. Phys. Chem.*, 2007, **58**, 267-297.
12. J. R. Anema, J.-F. Li, Z.-L. Yang, B. Ren and Z.-Q. Tian, *Annual Review of Analytical Chemistry*, 2011, **4**, 129-150.
13. K. Kim and H. S. Lee, *The Journal of Physical Chemistry B*, 2005, **109**, 18929-18934.
14. J. F. Li, Y. F. Huang, Y. Ding, Z. L. Yang, S. B. Li, X. S. Zhou, F. R. Fan, W. Zhang, Z. Y. Zhou and B. Ren, *nature*, 2010, **464**, 392-395.
15. J. M. Slocik and D. W. Wright, *Biomacromolecules*, 2003, **4**, 1135-1141.
16. D.-S. Wang and M. Kerker, *Physical Review B*, 1981, **24**, 1777.
17. E. J. Zeman and G. C. Schatz, *Journal of Physical Chemistry*, 1987, **91**, 634-643.
18. S. B. Chaney, S. Shanmukh, R. A. Dluhy and Y.-P. Zhao, *Applied Physics Letters*, 2005, **87**, 031908.
19. J. D. Driskell, S. Shanmukh, Y. Liu, S. B. Chaney, X.-J. Tang, Y.-P. Zhao and R. A. Dluhy, *The Journal of Physical Chemistry C*, 2008, **112**, 895-901.
20. Q. Liao, C. Mu, D.-S. Xu, X.-C. Ai, J.-N. Yao and J.-P. Zhang, *Langmuir*, 2009, **25**, 4708-4714.
21. B. McMillan, L. Berlouis, F. Cruickshank and P. Brevet, *Electrochimica Acta*, 2007, **53**, 1157-1163.
22. A. K. Oyelere, P. C. Chen, X. Huang, I. H. El-Sayed and M. A. El-Sayed, *Bioconjugate chemistry*, 2007, **18**, 1490-1497.
23. M. L. Pedano, S. Li, G. C. Schatz and C. A. Mirkin, *Angewandte Chemie*, 2010, **122**, 82-86.
24. S. Smitha, K. Gopchandran, T. Ravindran and V. Prasad, *Nanotechnology*, 2011, **22**, 265705.
25. J. Yao, G. Pan, K. Xue, D. Wu, B. Ren, D. Sun, J. Tang, X. Xu and Z. Tian, *Pure and applied chemistry*, 2000, **72**, 221-228.
26. S. Choi, M. Ahn and J. Kim, *Analytica chimica acta*, 2013, **779**, 1-7.
27. A. Garcia-Leis, J. V. Garcia-Ramos and S. Sanchez-Cortes, *The Journal of Physical Chemistry C*, 2013, **117**, 7791-7795.
28. K. A. Homan, J. Chen, A. Schiano, M. Mohamed, K. A. Willets, S. Murugesan, K. J. Stevenson and S. Emelianov, *Advanced functional materials*, 2011, **21**, 1673-1680.
29. B. Khlebtsov, E. Panfilova, V. Khanadeev and N. Khlebtsov, *Journal of Nanoparticle Research*, 2014, **16**, 1-12.
30. E. Nalbant Esenturk and A. Hight Walker, *Journal of Raman Spectroscopy*, 2009, **40**, 86-91.
31. A. Gutés, C. Carraro and R. Maboudian, *Journal of the American Chemical Society*, 2010, **132**, 1476-1477.
32. T. N. Huan, T. Ganesh, K. S. Kim, S. Kim, S.-H. Han and H. Chung, *Biosensors and Bioelectronics*, 2011, **27**, 183-186.
33. Z. Jiang, Y. Lin and Z. Xie, *Materials Chemistry and Physics*, 2012, **134**, 762-767.

34. Z.-Y. Lv, A.-Q. Li, Y. Fei, Z. Li, J.-R. Chen, A.-J. Wang and J.-J. Feng, *Electrochimica Acta*, 2013, **109**, 136-144.
35. Z.-Y. Lv, L.-P. Mei, W.-Y. Chen, J.-J. Feng, J.-Y. Chen and A.-J. Wang, *Sensors and Actuators B: Chemical*, 2014, **201**, 92-99.
36. N. D. Nikolic, K. I. Popov, L. J. Pavlovic and M. G. Pavlovic, *Sensors*, 2007, **7**, 1-15.
37. W. Song, Y. Cheng, H. Jia, W. Xu and B. Zhao, *Journal of colloid and interface science*, 2006, **298**, 765-768.
38. R.-C. Wang and C.-H. Li, *Acta Materialia*, 2011, **59**, 822-829.
39. S. Wang, L.-P. Xu, Y. Wen, H. Du, S. Wang and X. Zhang, *Nanoscale*, 2013, **5**, 4284-4290.
40. J. Xu, K. Yu and Z. Zhu, *Physica E: Low-dimensional Systems and Nanostructures*, 2010, **42**, 1451-1455.
41. W. Ye, Y. Chen, F. Zhou, C. Wang and Y. Li, *Journal of Materials Chemistry*, 2012, **22**, 18327-18334.
42. L. Cao, P. Diao, L. Tong, T. Zhu and Z. Liu, *ChemPhysChem*, 2005, **6**, 913-918.
43. B. Chen, G. Meng, Q. Huang, Z. Huang, Q. Xu, C. Zhu, Y. Qian and Y. Ding, *ACS applied materials & interfaces*, 2014, **6**, 15667-15675.
44. R. Contreras-Caceres, C. Dawson, P. Formanek, D. Fischer, F. Simon, A. Janke, P. Uhlmann and M. Stamm, *Chemistry of Materials*, 2013, **25**, 158-169.
45. Y. Cui, B. Ren, J.-L. Yao, R.-A. Gu and Z.-Q. Tian, *The Journal of Physical Chemistry B*, 2006, **110**, 4002-4006.
46. B. N. Khlebtsov, Z. Liu, J. Ye and N. G. Khlebtsov, *Journal of Quantitative Spectroscopy and Radiative Transfer*, 2015, **167**, 64-75.
47. Y. Ma, J. Zhou, W. Zou, Z. Jia, L. Petti and P. Mormile, *Journal of nanoscience and nanotechnology*, 2014, **14**, 4245-4250.
48. C. Song, J. L. Abell, Y. He, S. H. Murph, Y. Cui and Y. Zhao, *Journal of Materials Chemistry*, 2012, **22**, 1150-1159.
49. X. Chen, C. H. Cui, Z. Guo, J. H. Liu, X. J. Huang and S. H. Yu, *Small*, 2011, **7**, 858-863.
50. A. Gutés, R. Maboudian and C. Carraro, *Langmuir*, 2012, **28**, 17846-17850.
51. T. N. Huan, S. Kim, P. Van Tuong and H. Chung, *RSC Advances*, 2014, **4**, 3929-3933.
52. S. Kim, T. N. Huan, J. Kim, S. Y. Yoo and H. Chung, *Analytica Chimica Acta*, 2015, **885**, 132-139.
53. I. Najdovski, P. Selvakannan and A. P. O'Mullane, *RSC Advances*, 2014, **4**, 7207-7215.
54. X. Sun, L. Lin, Z. Li, Z. Zhang and J. Feng, *Materials Letters*, 2009, **63**, 2306-2308.
55. Z. Yi, S. Chen, Y. Chen, J. Luo, W. Wu, Y. Yi and Y. Tang, *Thin Solid Films*, 2012, **520**, 2701-2707.
56. Q.-X. Zhang, Y.-X. Chen, Z. Guo, H.-L. Liu, D.-P. Wang and X.-J. Huang, *ACS applied materials & interfaces*, 2013, **5**, 10633-10642.
57. M. Fernanda Cardinal, B. Rodríguez-González, R. A. Alvarez-Puebla, J. Pérez-Juste and L. M. Liz-Marzán, *The Journal of Physical Chemistry C*, 2010, **114**, 10417-10423.
58. J.-P. Lee, D. Chen, X. Li, S. Yoo, L. A. Bottomley, M. A. El-Sayed, S. Park and M. Liu, *Nanoscale*, 2013, **5**, 11620-11624.
59. G. Li, X. Song, Z. Sun, S. Yang, B. Ding, S. Yang, Z. Yang and F. Wang, *Solid State Sciences*, 2011, **13**, 1379-1384.

60. P.-F. Nan, X. Wang and X.-P. Qu, 2013.
61. B. Paramanik and A. Patra, *Journal of Materials Chemistry C*, 2014, **2**, 3005-3012.
62. S. Tang, S. Vongehr, Y. Wang, J. Cui, X. Wang and X. Meng, *Journal of Materials Chemistry A*, 2014, **2**, 3648-3660.
63. Y. Zhang, C. Wang, J. Wang, L. Chen, J. Li, Y. Liu, X. Zhao, Y. Wang and J. Yang, *Spectrochimica Acta Part A: Molecular and Biomolecular Spectroscopy*, 2016, **152**, 461-467.
64. T. T. B. Quyen, W.-N. Su, C.-H. Chen, J. Rick, J.-Y. Liu and B.-J. Hwang, *Journal of Materials Chemistry B*, 2014, **2**, 5550-5557.
65. B. Loganathan and B. Karthikeyan, *Colloids and Surfaces A: Physicochemical and Engineering Aspects*, 2013, **436**, 944-952.
66. B. Karthikeyan and B. Loganathan, *Materials Letters*, 2012, **85**, 53-56.
67. B. Karthikeyan and B. Loganathan, *Physica E: Low-dimensional Systems and Nanostructures*, 2013, **49**, 105-110.
68. M. Tsuji, M. Matsunaga, H. Kumagai, M. Ogino, S. Hikino, Y. Yoshida and T. Ishizaki, *CrystEngComm*, 2013, **15**, 1345-1351.
69. M. Tsuji, M. Matsunaga, Y. Yoshida, M. Hattori and T. Ishizaki, *CrystEngComm*, 2013, **15**, 7062-7070.
70. G. Zhang, S. Sun, M. Cai, Y. Zhang, R. Li and X. Sun, *Sci. Rep.*,2013, **3**, 1526.
71. J. N. Tiwari, K. C. Kemp, K. Nath, R. N. Tiwari, H. G. Nam and K. S. Kim, *ACS Nano*, 2013, 10, 9223–9231.
72. D. Cheng, X. Liu, D. Cao, W. Wang and S. Huang, *Nanotechnology*, 2007, **18**, 475702.
73. X. Wu, G. Wu, Y. Chen and Y. Qiao, *The Journal of Physical Chemistry A*, 2011, **115**, 13316-13323.

Figure Captions

Figure 1. SEM images of Cu flower-like structures formed by increasing the duration of electrodeposition: (3 (a), 5 (b), 7 (c), 10 (d), and 12 minutes (e). SEM image of the structure prepared with a 10 minute electrodeposition is shown in a larger field of view (f).

Figure 2. SEM images of Ag-Cu nanodendrite structures obtained by increasing the duration of GRR up to 15 minutes: 2 (a), **5 (b), 7 (c), 10 (d), 12 (e), and 15 minutes (g).**

Figure 3. Raman spectra of R6G (100 μM) acquired using six Ag-Cu nanodendrites (Fig. 2) prepared with increased duration of GRR up to 15 minutes. The strongest 1510 cm-1 peaks are highlighted (b) and the corresponding peak intensities are shown (c). The intensity of the same sample obtained using the Ag nanodendrite is added for comparison (c).

Figure 4. TEM image of the Ag-Cu nanodendrite (prepared with a 10 minute GRR), and the corresponding elemental mapping of Ag (b), and Cu (c).

Figure 5. Intensities of the 1510 cm-1 band acquired using Au-Ag-Cu nanodendrites constructed with different durations (5, 10, 15, 20, 25 s) of GRR (a). The intensity obtained using the Ag nanodendrite is added for comparison. SEM image of the Au-Ag-Cu nanodendrite constructed with a GRR over 15 s is shown (b).

Figure 6. TEM image of the Au-Ag-Cu nanodendrite (a) and the corresponding elemental mapping of Au (b), Ag (c), and Cu (d).

Figure 7. Peak intensities of a R6G sample (100 μM) at 1510 cm-1 acquired using the optimal Ag-Cu and Au-Ag-Cu nanodendrites over a period of 25 days (a) and Raman spectra of seven R6G samples (concentrations: 10-10 to 10-4 M) acquired using the optimal Au-Ag-Cu nanodendrite. The inset presents spectra corresponding to the two lowest concentration samples (10-9 and 10-10 M).

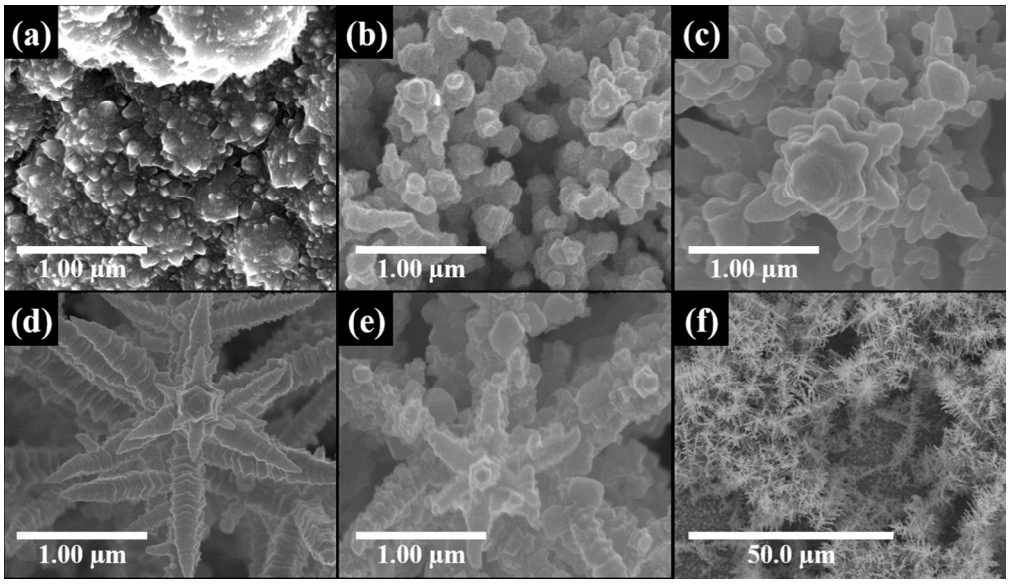

Figure 1. SEM images of Cu flower-like structures formed by increasing the duration of electrodeposition: (3 (a), 5 (b), 7 (c), 10 (d), and 12 minutes (e). SEM image of the structure prepared with a 10 minute electrodeposition is shown in a larger field of view (f).

245x140mm (150 x 150 DPI)

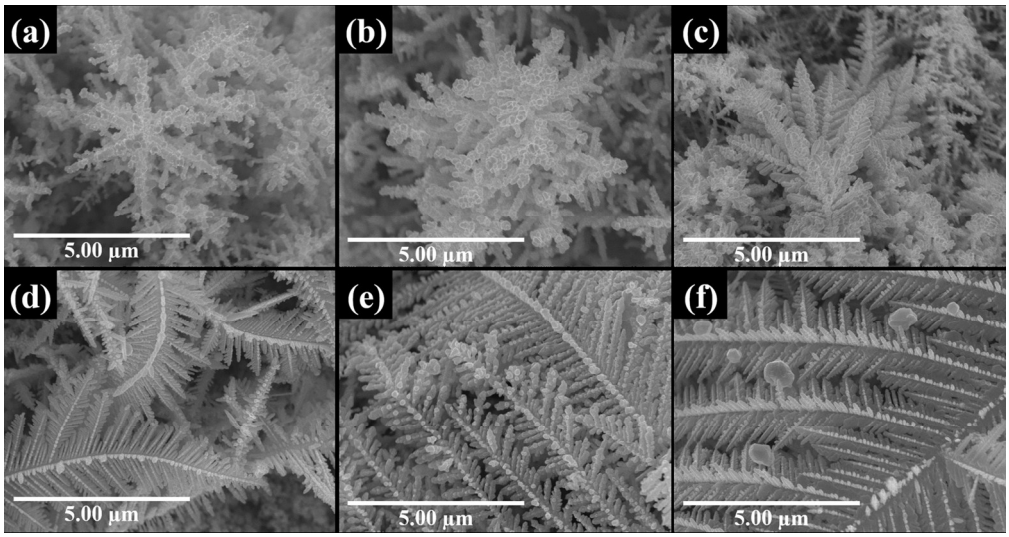

Figure 2. SEM images of Ag-Cu nanodendrite structures obtained by increasing the duration of GRR up to 15 minutes: 2 (a), 5 (b), 7 (c), 10 (d), 12 (e), and 15 minutes (g).

333x175mm (150 x 150 DPI)

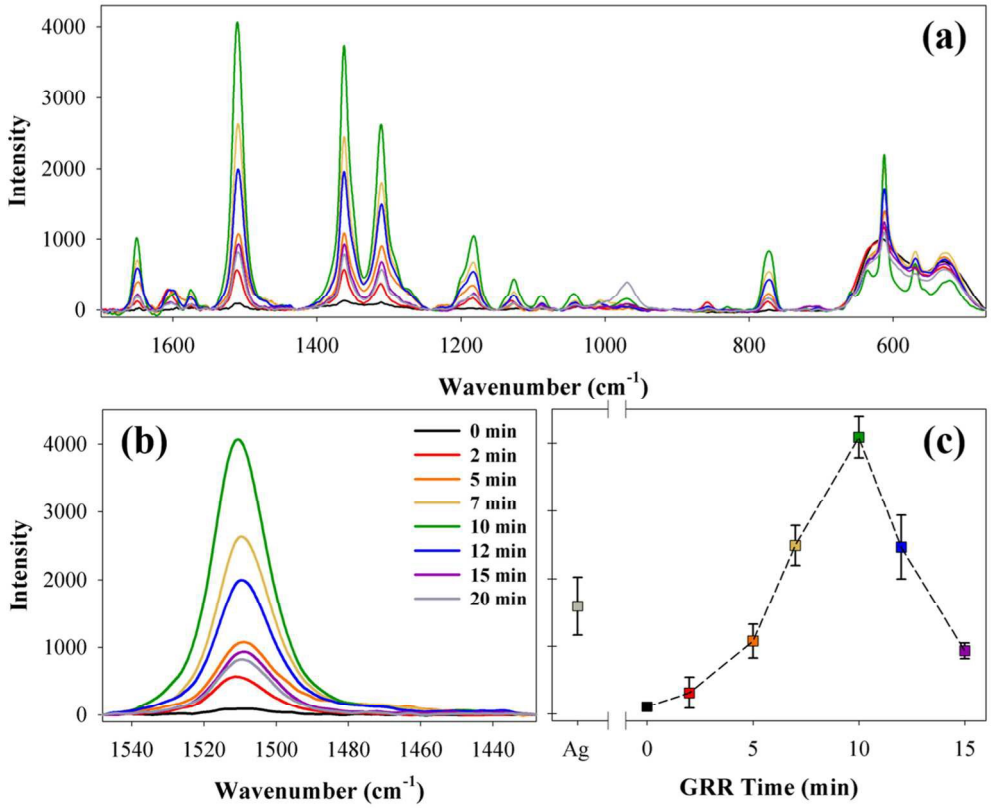

Figure 3. Raman spectra of R6G (100 μM) acquired using six Ag-Cu nanodendrites (Fig. 2) prepared with increased duration of GRR up to 15 minutes. The strongest 1510 cm-1 peaks are highlighted (b) and the corresponding peak intensities are shown (c). The intensity of the same sample obtained using the Ag nanodendrite is added for comparison (c).

224x183mm (150 x 150 DPI)

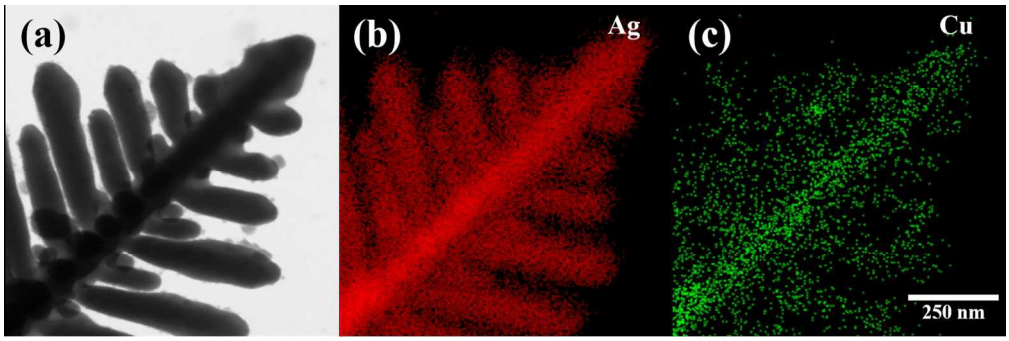

Figure 4. TEM image of the Ag-Cu nanodendrite (prepared with a 10 minute GRR), and the corresponding elemental mapping of Ag (b), and Cu (c).

318x105mm (150 x 150 DPI)

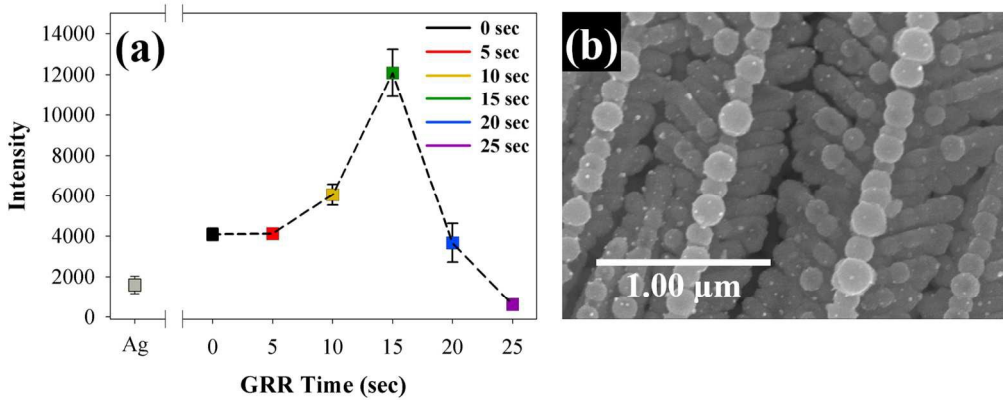

Figure 5. Intensities of the 1510 cm-1 band acquired using Au-Ag-Cu nanodendrites constructed with different durations (5, 10, 15, 20, 25 s) of GRR (a). The intensity obtained using the Ag nanodendrite is added for comparison. SEM image of the Au-Ag-Cu nanodendrite constructed with a GRR over 15 s is shown (b).

288x118mm (150 x 150 DPI)

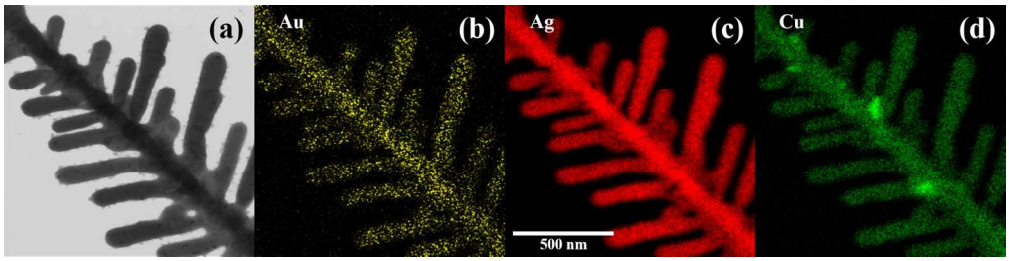

Figure 6. TEM image of the Au-Ag-Cu nanodendrite (a) and the corresponding elemental mapping of Au (b), Ag (c), and Cu (d).

335x84mm (150 x 150 DPI)

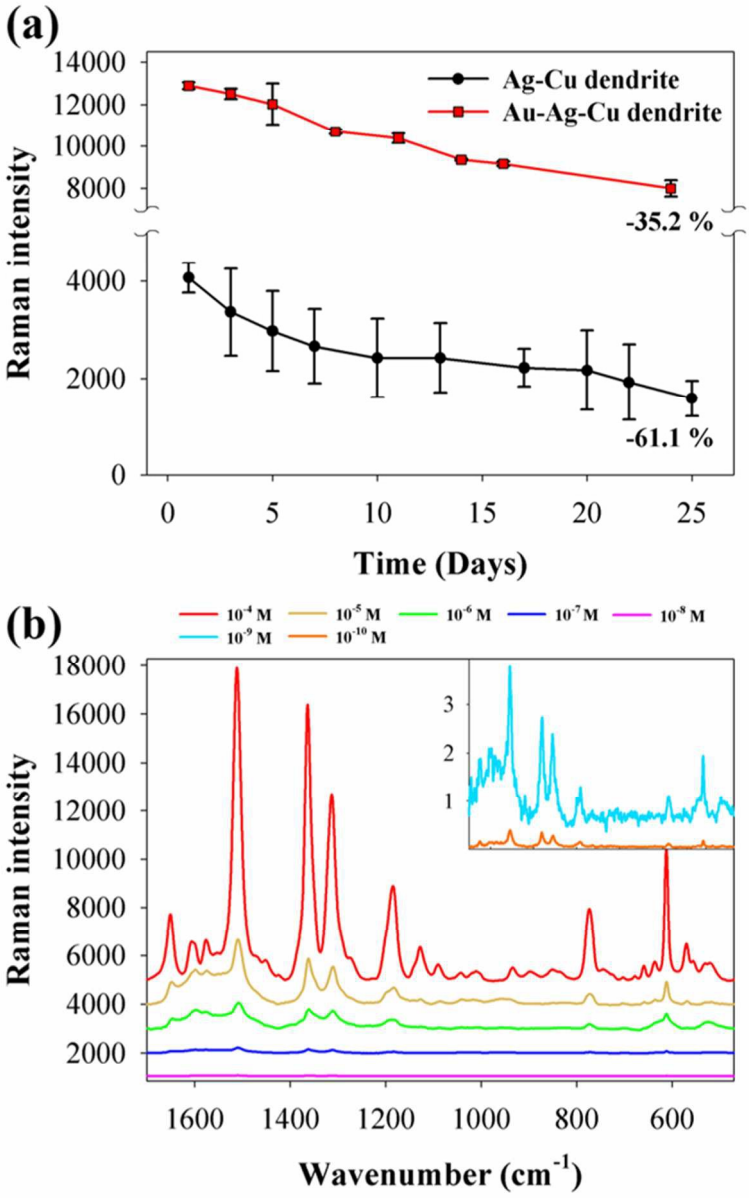

Figure 7. Peak intensities of a R6G sample (100 μM) at 1510 cm-1 acquired using the optimal Ag-Cu and Au-Ag-Cu nanodendrites over a period of 25 days (a) and Raman spectra of seven R6G samples (concentrations: 10-10 to 10-4 M) acquired using the optimal Au-Ag-Cu nanodendrite. The inset presents spectra corresponding to the two lowest concentration samples (10-9 and 10-10 M).

119x187mm (150 x 150 DPI)

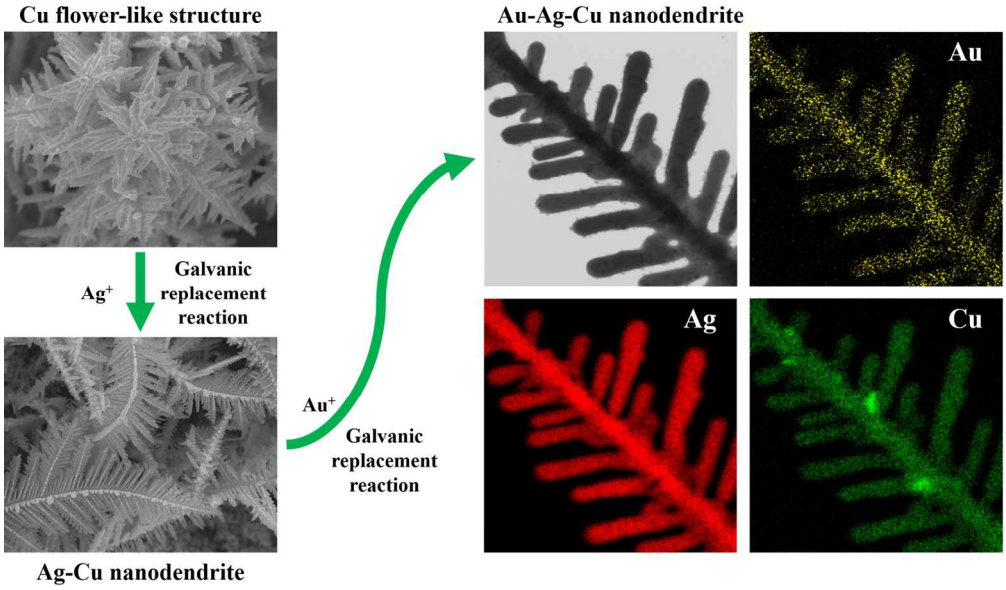

314x190mm (150 x 150 DPI)